



Nanoscale

1D Topological Phase in Transition-Metal Monochalcogenides Nanowires

Journal:	<i>Nanoscale</i>
Manuscript ID	NR-ART-05-2020-003529.R1
Article Type:	Paper
Date Submitted by the Author:	12-Jun-2020
Complete List of Authors:	Jin, Kyung-Hwan; University of Utah, Materials Science and Engineering Liu, Feng; University of Utah, Department of Materials Science

SCHOLARONE™
Manuscripts



1D Topological Phase in Transition-Metal Monochalcogenides Nanowires†

Received 00th January 20xx,
Accepted 00th January 20xx

Kyung-Hwan Jin,^{a,b,c} and Feng Liu^{c,*}

DOI: 10.1039/x0xx00000x

www.rsc.org/

The Su–Schrieffer–Heeger (SSH) model is a prototypical one-dimensional (1D) diatomic lattice model for non-trivial topological phase and topological excitations. Theoretically, many variations and extensions of the SSH model have been proposed and explored to better understand novel aspects of topological physics in low dimensions at nanoscale. However, the outstanding challenge remains to find real nanomaterials with robust structural stability for realizing the 1D topological states. Here, we develop an extended version of SSH model with multi-atomic bases of four, six and eight atoms and an imposed screw rotation symmetry. Furthermore, based on first-principles calculations, we demonstrate the realization of this model in transition metal monochalcogenides M_6X_6 ($M = \text{Mo}$ and W ; $X = \text{S}$, Se and Te) nanowires. The topological features of the doped M_6X_6 nanowires is confirmed with non-trivial edge modes and $e/2$ fractional charges, representative of the 1D non-trivial Zak phase. Our finding not only sheds new light on our fundamental understanding of 1D topological physics, but also significantly extends the scope of 1D topological materials that will attract immediate experimental interest, since isolated M_6X_6 nanowires have already been synthesized in experiments.

Introduction

The concept of topological order in condensed matter physics provides a new theme for understanding the origin of various quantum phases and has promoted intense recent interest in searching for nontrivial topological materials. The topological phase is characterized by global properties rather than a local order, making it very robust against local perturbations; this topological robustness makes emergent topological excitations a promising candidate for quantum computing and devices. Since the discovery of topological phases in the 1980s, comprehensive theoretical and experimental studies have been carried out to create, classify, and comprehend these exotic phases. Among the wide variety of topological models, the Su–Schrieffer–Heeger (SSH) model¹ serves as a paradigmatic model in describing band topology. The SSH model describes spin-less fermions hopping on a one-dimensional (1D) lattice with staggered hopping amplitudes. The Zak phase², i.e., Berry phase in 1D, is used to classify two

topologically distinct phases in the SSH model. The topological feature is characterized with zero energy states and fractionalized charges at the end of the non-trivial phase or domain walls between the two phases³⁻⁴.

One outstanding challenge is to realize 1D topological phases in nanomaterials with robust structural stability. The 1D topological phases have been demonstrated in recent experiments, using optical lattice⁵, cold atom⁶ or artificial lattice⁷ systems. But the electronic material platform for the SSH model is very rare. So far, the observation of increased conductivity due to soliton in polyacetylene^{1, 8} and the chiral solitons in indium wires self-assembled on the Si (111) surface⁹ has been considered indicative of 1D topological origin. However, polyacetylene is a polymer with weak structural stability, rendering measurement of topological edge mode difficult. The indium wires are formed on a substrate corresponding to a quasi 1D structure due to its interaction with the surface. Therefore, it is highly desirable to find isolated 1D system with strong structural stability for realization of topological properties.

1D metallic transition metal monochalcogenides (TMMs) nanowires, M_6X_6 ($M = \text{Mo}$ and W ; $X = \text{S}$, Se and Te), have shown structures and intrinsic anisotropic metallic properties as promising candidates for nanodevices. They have been theoretically studied¹⁰⁻¹³ and successfully synthesized both in isolated as well as crystal (bundle) forms¹⁴⁻²¹. For example, an isolated, nanometer-long M_6X_6 nanowire has been fabricated using electron-beam irradiation methods¹⁷⁻¹⁸. Isolated Mo_6Te_6 nanowires encapsulated in carbon nanotubes were also

^a Center for Artificial Low Dimensional Electronic Systems, Institute for Basic Science (IBS), Pohang 37673, Korea

^b Department of Physics, Pohang University of Science and Technology, Pohang 37673, Republic of Korea

^c Department of Materials Science and Engineering, University of Utah, Salt Lake City, UT 84112, United States

†Electronic Supplementary Information (ESI) available: Wannier function method, topological domain wall states of extended SSH model, topological edge modes of extended SSH models, metal-insulator transition depending on intra- and inter-hopping parameters, linear band of $\text{Mo}_6\text{Re}_2\text{X}_6$ nanowires, atomic structure of $\text{Mo}_6\text{S}_4\text{A}_2$ ($A = \text{Cl}$, Br and I) nanowire and band structures, Topological domain wall states of $\text{Mo}_6\text{Re}_2\text{S}_6$ nanowire, Correlation and strain effect in TMM nanowires. See DOI: 10.1039/x0xx00000x

*Corresponding author: fliu@eng.utah.edu

ARTICLE

Nanoscale

synthesized²¹. The fascinating properties of these single TMM nanowires are strong structural stability with a small diameter of about $\sim 9\text{\AA}$ and their tunable electronic properties by doping^{11-12, 22-23}.

Here, we demonstrate that the TMM nanowires offer an attractive new route to realizing 1D topological phases. We first develop an extended version of SSH model with multi-atomic bases. Dirac state at the zone-boundary is induced by using bases of four, six and eight atoms, instead of two atoms, and by imposing screw rotation symmetry along the axis of 1D system. Considering the dimerization due to the Peierls instability, a topological gap is opened at the Dirac point, leading to non-trivial edge modes at the boundary. Furthermore, based on first-principles calculation, we demonstrate the topological phase in the M_6X_6 nanowires are real materials to be represented by our extended SSH model with a six-atom basis. By doping the 1D TMMs nanowires with Re (Cl, Br and I) atom for transition metal (chalcogenides) atoms, the Dirac state can be adjust as to Fermi level, and meantime a Peierls distortion is induced. The resulting topological phase in the doped M_6X_6 nanowires is confirmed with non-trivial edge modes and $e/2$ fractional charges.

Methods

Structural and electronic properties of TMM nanowires are computed using the DFT scheme implemented in the Vienna ab initio simulation package (VASP) code²⁴. The projector-augmented-wave method is used to describe the ionic core-valence electron interactions²⁵. The generalized gradient approximation (GGA) is employed to describe the exchange and correlation potential²⁶. Spin-orbit coupling is included in all electronic structure calculations. Electronic wave functions are expanded in plane waves with an energy cutoff of 500 eV. To describe isolated nanowires while using periodic boundary conditions, we arranged the nanowires with a large interwire separation of 20 \AA . Geometries are optimized until the forces on each atom are less than 0.01 eV/ \AA . We used a $1 \times 1 \times 15$ k -point grid to sample the 1D Brillouin zone. An electronic-temperature smearing of 0.02 eV was employed for the occupation of the electronic states. We constructed Wannier representations by projecting the Bloch states from the first-principles bands of TMM nanowires onto M d and X p orbitals²⁷. Based on Wannier representations, we further calculated the Zak phase and the edge states of a semi-infinite system for topological properties²⁸⁻²⁹.

Results and discussion

Let's begin with the well-known SSH model in its the simplest form [Fig. 1(a)]. It consists of a chain of equally spaced atoms with s or p_z orbital. Considering the Peierls paring distortion, a topological phase transition occurs by tuning the ratio between inter- and intra-cell electron hoppings. If inter-cell hoppings are larger than the intra-cell hoppings, the Zak phase

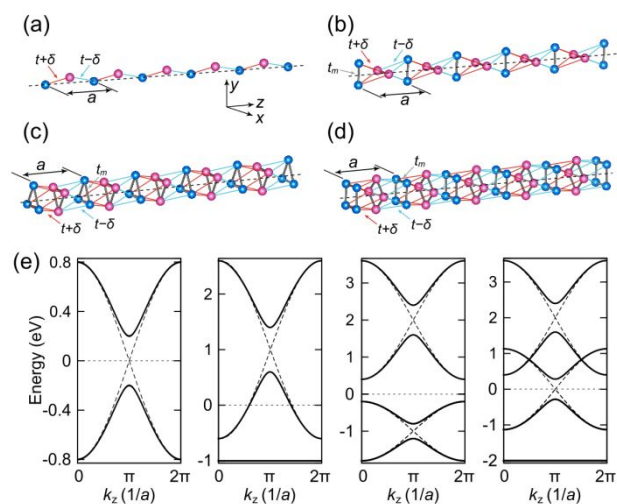


Fig. 1 Extended version of SSH model with multi-atomic bases. (a)-(d) 1D SSH model with two-, four-, six- and eight-atom bases, respectively. e Tight binding band structures from left to right for model a, b, c and d with parameters: $t=0.4$ eV, $t_m=1$ eV and $|\delta|=0.1$ eV, respectively. The dashed line represents the band structure without dimerization ($\delta=0$ eV).

emerges and edge states appear as a consequence of bulk-edge correspondence³⁰⁻³¹. Now, we replace each atom with a molecule, such as H_2 molecule or molecules with a ring configuration [Fig. 1(b)-(d)]. Specifically, in Fig. 1(b), the two atoms in the molecule are arranged in orientations perpendicular to each other, so that the whole system has time-reversal symmetry T and screw rotation symmetry $S_z=\{C_{4z}|0,0,1/2\}$; the latter combines a fourfold rotation and a half-lattice translation along the z axis. Similarly, for the other chain structures in Fig. 1(c) and 1(d), the screw rotation symmetry are $\{C_{6z}|0,0,1/2\}$ and $\{C_{8z}|0,0,1/2\}$, respectively. The Hamiltonian of these chain structures with multi-atom bases is given as follow:

$$H = \sum_{\langle i,j \rangle} t_{ij} c_i^\dagger c_j + t_m \sum_{[i,j]} c_i^\dagger c_j + h.c., \quad (1)$$

where $c_i^\dagger (c_i)$ is the creation (annihilation) operator of the i -th lattice. The first term represents the inter molecular hopping along the chain direction (z -direction) with the hopping parameter t_{ij} . There are two types of hopping along the z -direction, i.e., $t_{ij}=t+\delta$ and $t_{ij}=t-\delta$ to account for the Peierls distortion. The second term represents the intra hopping within the molecule, and the $[i,j]$ represents the hopping sites.

The energy spectra of the chain configurations in Fig. 1(a)-(d) are displayed in Fig. 1(e). Without dimerization, there are Dirac bands (dashed lines) crossing at the zone boundary ($k_z = \pi/a$), where a is the lattice period along the z -direction. Since the T commutes with S_z , $[T, S_z]=0$, it ensures the twofold band degeneracy, i.e., stability of Dirac point at $k_z = \pi/a$ point. When the Peierls distortion is included, this degeneracy is lifted to open a trivial or nontrivial gap depending on the sign of δ (or

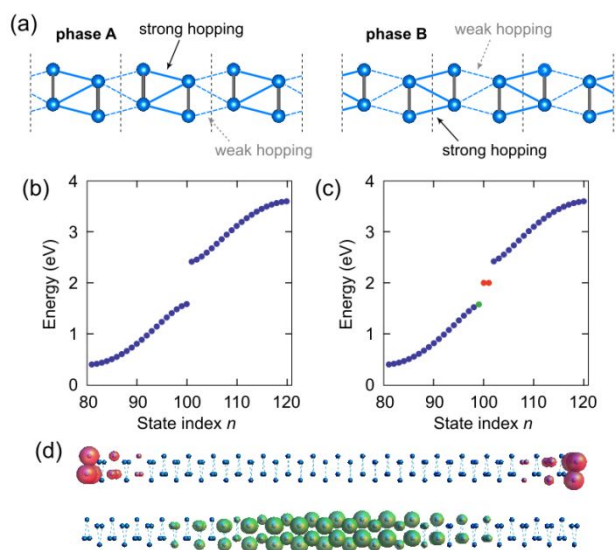


Fig. 2 Topological edge modes of extended SSH model. (a) The two phases in the extended SSH model with six-atom basis [Fig. 1(c)] where the strong hopping is either inside the unit cell (phase A) or between the unit cells (phase B). (b),(c) The calculated energy states of finite chain for phase A ($t=0.4$ eV, $t_m=1$ eV and $\delta=0.1$ eV) and phase B ($t=0.4$ eV, $t_m=1$ eV and $\delta=-0.1$ eV) in (a), respectively. The finite chain length is 20 times of unit cell. Topological edge states in phase B are marked as red dots in the topological gap, which are characterized by the π Zak phase accompanying a fractional charge $e/2$. (d) The spatial distribution of the edge states (red spheres) and bulk states (green spheres) as indicated in (c).

unit cell construction). The topological properties of 1D systems are characterized by the so-called Zak phase, i.e., the Berry phase picked up by a particle moving across the Brillouin zone². The Zak phase has been shown to be related to polarization³². The Zak phase of the n th band γ_n is integral over the Brillouin zone (BZ) of the Berry connection:

$$\gamma_n = i \int_{-G/2}^{G/2} \langle u_{nk} | \partial_k | u_{nk} \rangle dk, \quad (2)$$

where $|u_{nk}\rangle$ is the periodic part of the Bloch function of n th band with momentum k , and $G=2\pi/a$ is the reciprocal lattice vector. The total Zak phase, φ_{Zak} , for a given 1D insulator is the sum of γ_n over the occupied bands, i.e., $\varphi_{\text{Zak}} = \sum_n \gamma_n$. Once we obtain $|u_{nk}\rangle$ from first-principles calculation or tight-binding model Hamiltonians, we can evaluate φ_{Zak} by numerically integrating the Berry connection over the 1D BZ (see Supplementary Information[†]). The non-trivial Zak phases underlie the existence of protected edge states, fermion number fractionalization, and irrationally charged domain walls between topologically distinct 1D systems. When $\delta < 0$, φ_{Zak} is π and the system is topological nontrivial phase, whereas when $\delta > 0$, $\varphi_{\text{Zak}} = 0$ and the system is topologically trivial.

To further reveal the topological nature of the extended SSH model, we also calculated the edge states. The existence of zero modes with fractional charge is one of the key signatures of non-trivial Zak phase. Fig. 2(a) shows the two distinct Zak phases of the SSH model with six-atom basis for the opposite sign of δ . If the strong bond is

Table 1 Optimized lattice parameters [a and h are marked in Fig. 3(a) in unit of Å] of TMM nanowires, Fermi velocity (v_F in unit of 10^5 m/s), band gaps (E_g in unit of eV), and the reaction energies (ΔH in unit of eV) of Re-doped TMM nanowires.

	a	a_{exp}	h	v_F	E_g	ΔH
Mo ₆ S ₆	4.35	4.5 ^a	4.30	4.81	0.19	-1.39
Mo ₆ Se ₆	4.44	4.5 ^a	4.53	4.62	0.20	-1.42
Mo ₆ Te ₆	4.58	4.8 ^b	4.87	4.59	0.16	-1.36
W ₆ S ₆	4.37	4.4 ^a	4.35	5.99	0.18	-0.81
W ₆ Se ₆	4.46	-	4.59	5.73	0.18	-0.87
W ₆ Te ₆	4.56	-	4.95	5.26	0.01	-0.72

^aFrom Ref. 17. ^bFrom Ref. 21.

inside the unit cell (phase A), the system is trivial ($\varphi_{\text{Zak}}=0$). If the strong bond is located between the unit cells (phase B), it is a topological phase ($\varphi_{\text{Zak}}=\pi$). Fig. 2(b) and 2(c) shows the calculated energy states of finite chain for phase A and B, respectively. The finite chain is constructed by 20 times of the unit cell. For the trivial phase, there are no zero-energy edge states in the bulk gap. In contrast topological edge states marked as red dots appear in the topological gap in Fig. 2(c), which are characterized by a π Zak phase accompanying a fractional charge $e/2$ at the end of chain. Furthermore, the topological domain-wall states appear between phase A and phase B (see supplementary Fig. S1[†]). Therefore, these results demonstrate that the extended SSH model can indeed exhibit topological state. Other multi-atom-basis models also show topological edge modes in the bulk gap (see Fig. S2-S4[†]).

Next, we demonstrate a real material system to realize the newly developed extended 1D SSH model. The 1D topological material should meet the following conditions: (i) An alternating arrangement of molecular structure with screw rotation symmetry; (ii) A Dirac point is isolated from other bands and located at Fermi level. Specifically, we narrow down our search to transition-metal monochalcogenides (TMMs), which have a common formula M_6X_6 , where M is a transition metal atom (Mo, W) and X is a chalcogen atom (S, Se, Te). As illustrated in Fig. 3(a), M_6X_6 nanowires are 1D materials comprised of alternately stacked M_3X_3 triangles along the wire axis, with three capping X atoms located at the vertices of the triangles and three M atoms located between the X atoms. The structure contains the screw rotation symmetry $S_2=\{C_{6z}|0,0,1/2\}$. Thus, their structure satisfies the first condition. Their optimized lattice parameters are presented in Table 1, consistent with previous works^{10, 13, 17, 21}.

Figure 3(b) and 3(c) show the calculated band structures of M_6X_6 nanowires. M_6S_6 and M_6Se_6 nanowires show metallic character, whereas M_6Te_6 is insulating. The metal-insulator transition can be explained by the TB model. In Eq. (1), there are two hopping parameters: one is the inter-molecular hopping t and the other is the intra-molecular hopping t_m . If $t > t_m/2$, the 1D system is metallic, while if $t < t_m/2$, the system turns to be insulating. As the halogen atomic mass increases, t is decreased turning metallic bands into insulating state (see supplementary Fig. S5[†]). All the bands near the Fermi level are contributed from the d orbitals of the transition-

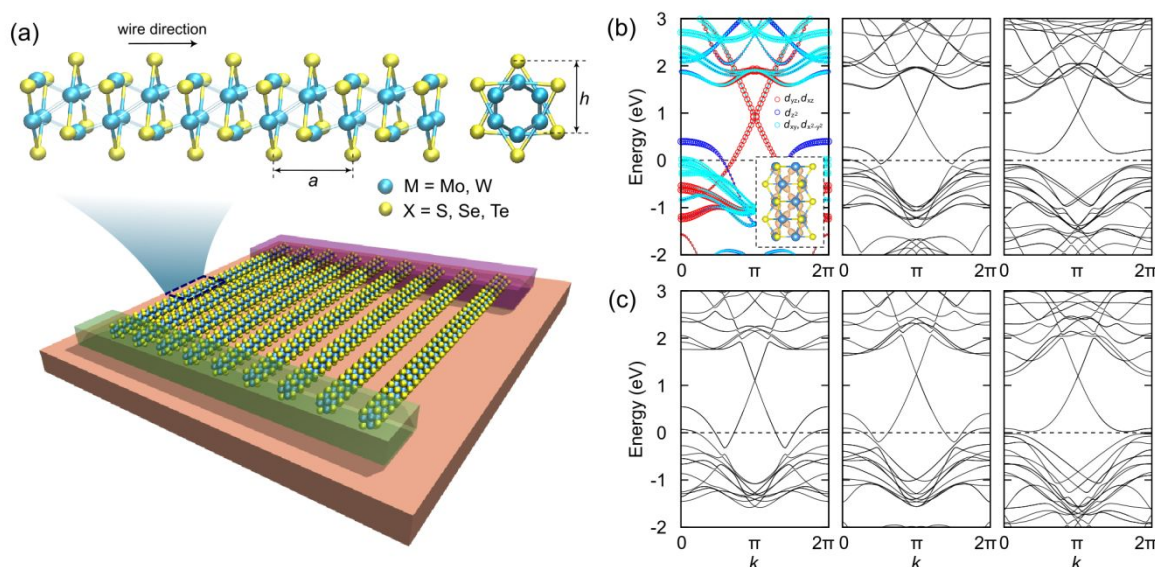
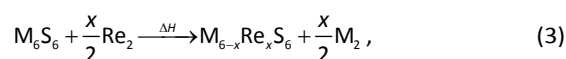


Fig. 3 Electronic structure of TMM nanowires. (a) Atomic structure of the M_6X_6 nanowire and schematic setup of transport measurement of TMM nanowires. (b) The calculated band structure of Mo_6S_6 (left), Mo_6Se_6 (middle) and Mo_6Te_6 (right) nanowire, respectively. Inset in the left panel shows the partial charge density of Dirac state. (c) The calculated band structure of W_6S_6 (left), W_6Se_6 (middle) and W_6Te_6 (right) nanowire, respectively.

metal (Mo or W) atoms. Interestingly, all the M_6X_6 nanowires have a hole-doped Dirac band, with the Dirac point at the zone boundary ($k_z = \pi/a$) point located above the Fermi level ~ 1 eV. These Dirac states are mainly originated from d_{xz} and d_{yz} orbitals of transition-metal atoms [see left panel of Fig. 3(b)]. The Dirac state has a Fermi velocity (v_F) of about $4.6\sim 4.8\times 10^5$ m/s and $5.3\sim 6.0\times 10^5$ m/s for Mo_6X_6 and W_6X_6 nanowires, respectively (Table 1), which is comparable to graphene³³ and edge states of quantum spin Hall insulators^{34–36}.

To realize the topological phase, the Dirac point needs to be moved to the Fermi level, in order to meet the second condition. Then, the band will be half-filled and $2k_F$ phonons of 1D lattice will be condensed to induce a lattice distortion with period $\lambda=1/2k_F$, known as the Peierls instability³⁷. In doing so, the electrons gain energy via dimerization that opens a gap at the Dirac point. Therefore, electron doping is needed, and specifically two electrons per unit cell, since there are two degenerate bands in between the Fermi level and Dirac point gap. This can be achieved by using Re atom as an electron donor to substitute 1/3 of transition metal atoms. It is worth noting that the Re-doped 2D transition metal dichalcogenides (TMDs) such as MX_2 (MoS_2 , $MoSe_2$, etc.) have been successfully synthesized by a facile hydrothermal reaction and an annealing process^{38–42}. Also it is reported that doping of TMDs with elements from Groups V–VII energetically favors substitutional doping instead of dopants occupying interstitial or defect sites³⁸. To test the feasibility of the electron doping, we have replaced one of the transition metal atoms in the stacked M_3X_3 triangles with Re atom to form $M_4Re_2X_6$. Then, one may consider the reaction energy ΔH of the substitution reaction



The reaction energies of all the checked $M_4Re_2X_6$ nanowires are presented in Table 1. Clearly, the desired reaction is exothermic for $x=2$, confirming its feasibility. Moreover, it is reported that $Mo_6S_{6-x}I_x$ nanowires with $x=2$ is particularly stable and rigid with the metallic linear band¹¹. A separate use of the doped $M_4Re_2X_6$ nanowires as a building block for device application is its 1D Dirac state with good conductance [see Fig. 3(a) and supplementary Fig. S6[†]]. All doped-TMM nanowires are metallic with a constant density of states near Fermi level, we can observe quantized conductance in the transport measurement.

The electron doping induces the Peierls distortion resulting in M–M bond distances. Fig. 4a shows the two phases of Re-doped Mo_6S_6 ($Mo_4Re_2S_6$) nanowires. The two different Mo–Mo bonding distances are 2.67 Å (short) vs. 2.71 Å (long). Depending on the unit cell construction, there are two different topologically distinct phases. For the phase A (B), the strong (weak) bond is inside the unit cell. Fig. 4(b) and 4(c) show the calculated band structures for $Mo_4Re_2X_6$ and $W_4Re_2X_6$, respectively. Without dimerization, the Dirac point is located at the Fermi level with the half-filled band. Due to the Peierls instability, the dimer formation of lower symmetry is found to be more energetically stable. The induced gaps of all the checked $M_4Re_2X_6$ nanowires are presented in Table 1. The gap size is ~ 0.2 eV for all the Re-doped TMM wires except for $W_4Re_2Te_6$ which has an additional band near the Fermi level. Due to the additional band near the Fermi level, the condition for the Peierls instability is not satisfied and the dimer formation does not appear in $W_4Re_2Te_6$ nanowire. We note that the dimer formation and the gap opening also found in the halogen-doped TMM nanowires, such as $Mo_6S_4Cl_2$, $Mo_6S_4Br_2$ and $Mo_6S_4I_2$ (see supplementary Fig. S7[†]). The topological

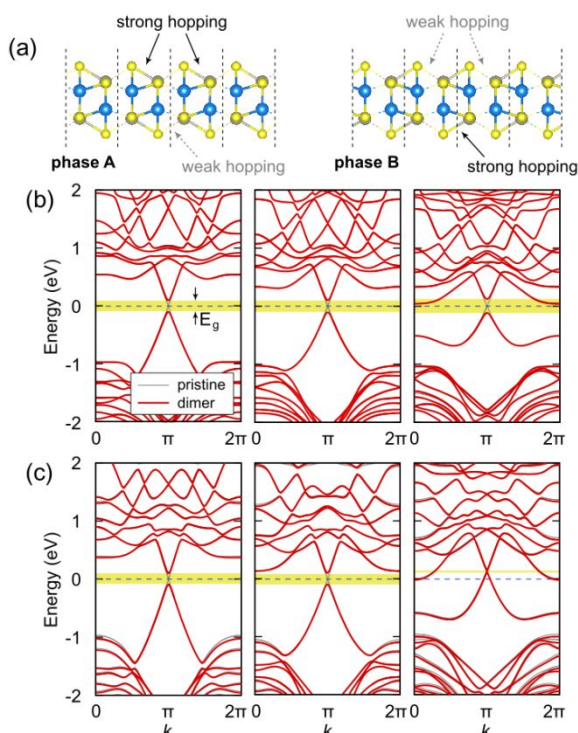


Fig. 4 1D topological phases in doped TMM nanowire. (a) The two phases of the $\text{Mo}_4\text{Re}_2\text{S}_6$ nanowire. (b) The calculated band structure of $\text{Mo}_4\text{Re}_2\text{X}_6$ (from left to right, $X=\text{S}, \text{Se}$ and Te) nanowires. An energy gap (E_g) is opened at the Dirac point due to the dimerization. The red (gray) line indicates bands of the dimerized (pristine) TMM nanowire. (c) The calculated band structure of $\text{W}_4\text{Re}_2\text{X}_6$ (from left to right, $X=\text{S}, \text{Se}, \text{Te}$) nanowires.

physics of Re-doped nanowires is further characterized by Zak phase. We have evaluated the φ_{Zak} for the occupied bands. The distinct topological character of the two phases is reflected in the difference of their Zak phases, $\Delta\varphi_{\text{Zak}}$. The calculated difference of Zak phase $\Delta\varphi_{\text{Zak}} = \varphi_{\text{Zak}}^{\text{A}} - \varphi_{\text{Zak}}^{\text{B}}$ is exactly π . Therefore the two differently dimerized TMM nanowires therefore belong to different topological classes.

The significant topological manifestation of non-trivial Zak phase is the emergence of the zero-energy modes in the bulk gap. We constructed a finite size of $\text{Mo}_4\text{Re}_2\text{S}_6$ nanowire by expanding the unit cell of phase B 10, 20 and 30 times. Fig. 5(a) shows their calculated edge states, respectively. Two in-gap topological edge states are found at the Fermi level. To compare phase A and B, we further calculated energy spectra of the semi-infinite nanowire in Fig. 5(b). For phase A, topological edge mode does not exist in the gap whereas phase B shows clear topological edge modes in the bulk gap. The real-space charge density distributions of edge and bulk states are shown in Fig. 5(c), respectively. The topological end state states are localized at the end of $\text{Mo}_4\text{Re}_2\text{S}_6$ nanowire and decay very quickly away from each edge with no overlap. The existence of a zero level leads to a half charge confined on the boundary of insulating nanowire. However, the bulk state, as indicated in Fig. 5(a), is distributed over the whole nanowire. Also,

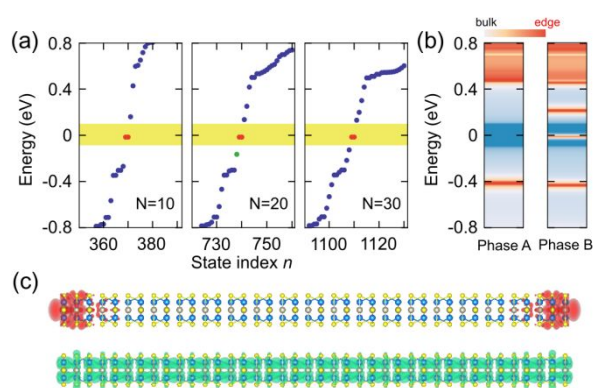


Fig. 5 The topological end state of TMM nanowire. (a) The calculated discrete energy levels of finite $\text{Mo}_4\text{Re}_2\text{S}_6$ nanowires (phase B) of with three different sizes. N is the number of unit cells, denoting the length of nanowire. Topological edge states in the bulk gap (yellow shaded) are indicated by red dots. Each state is doubly degenerated. (b) The edge spectral weight for phase A and B of semi-infinite $\text{Mo}_4\text{Re}_2\text{S}_6$ nanowire, respectively. (c) The real-space charge distribution of topological edge states and bulk state indicated by red and green dots in the middle panel of (a), respectively. The red (green) isosurface indicates the edge (bulk) states.

the topological zero-energy states are observed in the domain walls between two different Zak phases (see supplementary Fig. S8[†]).

For 1D TMM nanowires, one may wonder if the correlation effect of d electrons of transition metal elements would influence the topological properties. So we have investigated the correlation effects of d electrons in Mo_6S_6 and $\text{Mo}_4\text{Re}_2\text{S}_6$ by employing the GGA+U approach (with the onsite Hubbard U term). Using different U values from 0 to 4 eV for Mo and Re atoms, we found that both systems remain the nonmagnetic ground state and their nontrivial topological properties persist (see supplementary Fig. S9[†]).

We also studied the effect of uniaxial strain on the electronic/topological properties of the TMM nanowires. We checked the stability of $\text{Mo}_4\text{Re}_2\text{S}_6$ nanowire as a function of tensile strain (see supplementary Fig. S10[†]). The TMM nanowires remain stable up to 6% tensile strains without breaking. Most importantly, the topological energy gap induced by Peierls-dimerization is also preserved. With the increasing tensile strain, the gap at the X point increases. Above $\sim 4\%$ strain, the conduction band minimum at Γ point begins to descend gradually; however, the nontrivial topology remains.

Finally, we extend our discussion to the experimental feasibility of topological modes in 1D TMM nanowire. The Re doped M_6X_6 nanowire is described by Peierls-dimerized chain with two degenerated ground phases, i.e., A and B phase, which would appear with equal probability. Therefore, one

may expect that upon the phase transition, the dimers will form along the chain direction with both phases present and naturally there will be domain walls (stacking faults) in between two different phases. These topological boundary modes can be mobile, but are occasionally trapped by structural defects or impurities. Consequently, the oppositely charged topological end modes⁹, as trapped by defects, experience Coulomb attraction, which would shrink the size of a trapped soliton significantly⁴³. The topological boundary or end modes trapped by defects can be resolved through STM and STS measurements.

Conclusions

In conclusion, an extended 1D SSH model is theoretically developed and used to elucidate the 1D topological phase in transition metal monochalcogenides nanowires, as predicted by first-principle calculations of non-trivial Zak phase and in-gap topological edge states. Because the transition metal monochalcogenides nanowires have already been synthesized in experiments, we envision that our results will draw immediate experimental attention to detect the exotic 1D topological states in real materials. Moreover, other promising material platforms might be searched for based on the newly developed extended 1D SSH model, such as Van der Waals-wired materials and group-IV metal chalcogenide nanowires.

Acknowledgements

K.J acknowledges the support from Korea Research Fellowship Program through the National Research Foundation of Korea (NRF) funded by the Ministry of Science and ICT (Grant No. 2019H1D3A1A01071056) and the Institute for Basic Science (Grant No. IBS-R014-D1). F. Liu acknowledges financial support from DOE-BES (No. DE-FG02-04ER46148).

Conflicts of interest

There are no conflicts to declare.

References

1. W. P. Su, J. R. Schrieffer and A. J. Heeger, *Phys. Rev. Lett.*, 1979, **42**, 1698-1701.
2. J. Zak, *Phys. Rev. Lett.*, 1989, **62**, 2747-2750.
3. R. Jackiw and C. Rebbi, *Phys. Rev. D*, 1976, **13**, 3398-3409.
4. A. J. Heeger, S. Kivelson, J. R. Schrieffer and W. P. Su, *Rev. Mod. Phys.*, 1988, **60**, 781-850.
5. M. Atala, M. Aidelsburger, J. T. Barreiro, D. Abanin, T. Kitagawa, E. Demler and I. Bloch, *Nat. Phys.*, 2013, **9**, 795-800.
6. E. J. Meier, F. A. An and B. Gadway, *Nat. Commun.*, 2016, **7**, 13986.
7. R. Drost, T. Ojanen, A. Harju and P. Liljeroth, *Nat. Phys.*, 2017, **13**, 668-671.
8. C. K. Chiang, C. R. Fincher, Y. W. Park, A. J. Heeger, H. Shirakawa, E. J. Louis, S. C. Gau and A. G. MacDiarmid, *Phys. Rev. Lett.*, 1977, **39**, 1098-1101.
9. S. Cheon, T.-H. Kim, S.-H. Lee and H. W. Yeom, *Science*, 2015, **350**, 182-185.
10. D. Çakır, E. Durgun, O. Gülseren and S. Ciraci, *Phys. Rev. B*, 2006, **74**, 235433.
11. I. Popov, T. Yang, S. Berber, G. Seifert and D. Tománek, *Phys. Rev. Lett.*, 2007, **99**, 085503.
12. P. Murugan, V. Kumar, Y. Kawazoe and N. Ota, *Nano Lett.*, 2007, **7**, 2214-2219.
13. D. F. Souza, A. L. Rosa, P. Venezuela, J. E. Padilha, A. Fazio and R. B. Pontes, *Phys. Rev. B*, 2019, **100**, 235416.
14. L. Venkataraman and C. M. Lieber, *Phys. Rev. Lett.*, 1999, **83**, 5334-5337.
15. L. Venkataraman, Y. S. Hong and P. Kim, *Phys. Rev. Lett.*, 2006, **96**, 076601.
16. J. Kibsgaard, A. Tuxen, M. Levisen, E. Lægsgaard, S. Gemming, G. Seifert, J. V. Lauritsen and F. Besenbacher, *Nano Lett.*, 2008, **8**, 3928-3931.
17. J. Lin, O. Cretu, W. Zhou, K. Suenaga, D. Prasai, K. I. Bolotin, N. T. Cuong, M. Otani, S. Okada, A. R. Lupini, J.-C. Idrobo, D. Caudel, A. Burger, N. J. Ghimire, J. Yan, D. G. Mandrus, S. J. Pennycook and S. T. Pantelides, *Nat. Nanotech.*, 2014, **9**, 436-442.
18. A. L. Koh, S. Wang, C. Ataca, J. C. Grossman, R. Sinclair and J. H. Warner, *Nano Lett.*, 2016, **16**, 1210-1217.
19. H. Zhu, Q. Wang, C. Zhang, R. Addou, K. Cho, R. M. Wallace and M. J. Kim, *Adv. Mater.*, 2017, **29**, 1606264.
20. Y. Yu, G. Wang, Y. Tan, N. Wu, X.-A. Zhang and S. Qin, *Nano Lett.*, 2018, **18**, 675-681.
21. M. Nagata, S. Shukla, Y. Nakanishi, Z. Liu, Y.-C. Lin, T. Shiga, Y. Nakamura, T. Koyama, H. Kishida, T. Inoue, N. Kanda, S. Ohno, Y. Sakagawa, K. Suenaga and H. Shinohara, *Nano Lett.*, 2019, **19**, 4845-4851.
22. V. Nicolosi, P. D. Nellist, S. Sanvito, E. C. Cosgriff, S. Krishnamurthy, W. J. Blau, M. L. H. Green, D. Vengust, D. Dvorsek, D. Mihailovic, G. Compagnini, J. Sloan, V. Stolojan, J. D. Carey, S. J. Pennycook and J. N. Coleman, *Adv. Mater.*, 2007, **19**, 543-547.
23. T. Yang, S. Okano, S. Berber and D. Tománek, *Phys. Rev. Lett.*, 2006, **96**, 125502.
24. G. Kresse and J. Furthmüller, *Phys. Rev. B*, 1996, **54**, 11169-11186.
25. P. E. Blöchl, *Phys. Rev. B*, 1994, **50**, 17953-17979.
26. J. P. Perdew, K. Burke and M. Ernzerhof, *Phys. Rev. Lett.*, 1996, **77**, 3865-3868.
27. A. A. Mostofi, J. R. Yates, Y.-S. Lee, I. Souza, D. Vanderbilt and N. Marzari, *Comp. Phys. Commun.*, 2008, **178**, 685-699.
28. M. P. L. Sancho, J. M. L. Sancho and J. Rubio, *J. Phys. F*, 1984, **14**, 1205.
29. Q. Wu, S. Zhang, H.-F. Song, M. Troyer and A. A. Soluyanov, *Comput. Phys. Commun.*, 2018, **224**, 405-416.
30. X.-L. Qi and S.-C. Zhang, *Rev. Mod. Phys.*, 2011, **83**, 1057-1110.

31. J.-W. Rhim, J. Behrends and J. H. Bardarson, *Phys. Rev. B*, 2017, **95**, 035421.
32. R. D. King-Smith and D. Vanderbilt, *Phys. Rev. B*, 1993, **47**, 1651-1654.
33. D. C. Elias, R. V. Gorbachev, A. S. Mayorov, S. V. Morozov, A. A. Zhukov, P. Blake, L. A. Ponomarenko, I. V. Grigorieva, K. S. Novoselov, F. Guinea and A. K. Geim, *Nat. Phys.*, 2011, **7**, 701-704.
34. Z. F. Wang, L. Chen and F. Liu, *Nano Lett.*, 2014, **14**, 2879-2883.
35. K.-H. Jin and S.-H. Jhi, *Phys. Chem. Chem. Phys.*, 2016, **18**, 8637-8642.
36. K.-H. Jin, S.-H. Jhi and F. Liu, *Nanoscale*, 2017, **9**, 16638-16644.
37. R. E. Peierls, *Clarendon, Oxford*, 1955.
38. V. Kochat, A. Apte, J. A. Hachtel, H. Kumazoe, A. Krishnamoorthy, S. Susarla, J. C. Idrobo, F. Shimojo, P. Vashishta, R. Kalia, A. Nakano, C. S. Tiwary and P. M. Ajayan, *Adv. Mater.*, 2017, **29**, 1703754.
39. R. Mukherjee, H. J. Chuang, M. R. Koehler, N. Combs, A. Patchen, Z. X. Zhou and D. Mandrus, *Phys. Rev. Appl.*, 2017, **7**, 034011.
40. B. Xia, P. Liu, Y. Liu, D. Gao, D. Xue and J. Ding, *Appl. Phys. Lett.*, 2018, **113**, 013101.
41. K. Zhang, B. M. Bersch, J. Joshi, R. Addou, C. R. Cormier, C. Zhang, K. Xu, N. C. Briggs, K. Wang, S. Subramanian, K. Cho, S. Fullerton-Shirey, R. M. Wallace, P. M. Vora and J. A. Robinson, *Adv. Funct. Mater.*, 2018, **28**, 1706950.
42. M. Mandal, S. Marik, K. P. Sajilesh, Arushi, D. Singh, J. Chakraborty, N. Ganguli and R. P. Singh, *Phys. Rev. Mater.*, 2018, **2**, 094201.
43. W. P. Su, J. R. Schrieffer and A. J. Heeger, *Phys. Rev. B*, 1980, **22**, 2099-2111.

